Microgonotropens and Their Interactions with DNA. 3.[1] Structural Analysis of the 1:1 Complex of d(CGCAAATTTGCG)$_2$ and Dien-Microgonotropen-c by 2D NMR Spectroscopy and Restrained Molecular Modeling

Andrei Blaskó, Kenneth A. Browne, Gong-Xin He, and Thomas C. Bruice*

Contribution from the Department of Chemistry, University of California, Santa Barbara, California 93106

Received August 5, 1992

Abstract: The solution structures of d(CGCAAATTTGCG)$_2$ and the 1:1 complex of d(CGCAAATTTGCG)$_2$ with dien-microgonotropen-c (**5c**) have been determined by 1D and 2D ^{1}H NMR spectroscopy and restrained molecular modeling. One hundred and two resonances for the free DNA and 196 for the DNA bound to **5c** have been assigned. The 1D (DNA imino protons) and 2D (NOESY) spectra of the 1:1 complex show that there is an asymmetric type of binding in the A+T-rich region involving five base pairs (5′-$A_6T_7T_8T_9G_{10}$). The two most stable structures of the d(CGCAAATTTGCG)$_2$:**5c** complex have (i) pyrrole rings A and B coplanar and in the minor groove with pyrrole ring C out of plane by ~70° and (ii) pyrrole rings A, B, and C coplanar and in the minor groove. The amino terminal acetamide head is directed toward A_6 while the carboxy terminal (dimethylamino)propyl tail is directed toward and above G_{10}. The energy barrier between the two bound **5c** conformations is 2.5 kcal/mol in favor of the structure with only two pyrrole rings in the minor groove. The dien polyamino substituent residing on the nitrogen of pyrrole ring C runs above and along the phosphate backbone, toward the major groove. The protonated terminal dimethylamine nitrogen of the (dimethylamino)propyl tail is adjacent to a negatively charged phosphodiester linkage (P_{11}) on the minor groove side, while the protonated dien nitrogens reside on the edge of the major groove and pair with the phosphodiester linkages P_8, P_9, and P_{10}. The off-rate of **5c** from the 1:1 complex was found to be 1.3 ± 0.2 s^{-1}, corresponding to an activation energy of 17 kcal/mol. The relative positions of the DNA proton signals change as **5c** binds to the DNA. This is due, in part, to the widening of the minor groove (up to 3 Å) in the binding site. Compound **5c** binds 5–7 Å from the bottom of the groove and 5–6 and 4–6 Å distant from the (–) and (+) strands, respectively. Comparisons with the crystallographic data of the same DNA with and without distamycin were made. Molecular modeling of the free and **5c**-bound DNA, based on NOE measurements, shows that there is a break in the C_{2v} symmetry of the crystallized DNA at the A_6T_7 junction as it goes into aqueous solution. An increase in the helical bend of 10.6° from that of the crystallized DNA was found to occur in the solution DNA while an increase of only 6.4° was found for the solution DNA:**5c** complex relative to the crystallized dodecamer. Upon solvation, the length of the duplex increases by 0.1 Å/bp for both the dodecamer and the **5c**-complexed dodecamer compared to the case of crystal structures of free DNA and distamycin-complexed DNA.

Introduction

As a complementary tool to X-ray crystallography, two-dimensional (2D) ^{1}H NMR spectroscopy is the most important method for DNA structural analysis. Protons are excellent markers for monitoring base pairing and stacking, sugar puckering, and glycosidic torsion angles in nucleic acids, as well as in DNA–ligand interactions.[3] Ligands which recognize and bind to DNA, and which can be equipped with chemical or photochemical tags capable of modifying or cleaving DNA, have great prospects as "synthetic restriction enzymes" and as gene-selective drugs.[4] Oligonucleotides, able to recognize DNA with high fidelity via the formation of triple helices, have been widely studied.[5] Also, low molecular weight agents able to fit isohelically into the minor groove have been isolated or designed, and their complexes with DNA fragments have been characterized in solution (2D NMR)[6] or in solid state (X-ray crystallography and solid NMR).[7] Naturally occurring hybrid molecules with bimodal binding (intercalation and groove binding) and sequence-specific recognition abilities (actinomycin, doxorubicin, daunomycin, nogalamycin, arugomycin, dynemicin A, and neocarzinostatin)[5] provide models for the design of ligands exhibiting mixed modes of binding.

(1) Chemistry of Phosphodiesters, DNA and Models. 5. Part 1: Reference 2a. Part 2: Reference 2b. Part 3: Reference 8a. Part 4: Reference 8b.

(2) (a) Bruice, T. C.; Mei, H.-Y.; He, G.-X.; Lopez, V. *Proc. Natl. Acad. Sci.* U.S.A. **1992**, *89*, 1700. (b) Browne, K. A.; Bruice, T. C. *J. Am. Chem. Soc.* **1992**, *114*, 4951.

(3) (a) Patel, D. J.; Shapiro, L.; Hare, D. *Q. Rev. Biophys.* **1987**, *20*, 35. (b) Gao, X.; Patel, D. J. *Q. Rev. Biophys.* **1989**, *22*, 93. (c) Patel, D. J.; Shapiro, L. *Biochimie* **1985**, *67*, 887. (d) Patel, D. J.; Shapiro, L. *J. Biol. Chem.* **1986**, *261*, 1230.

(4) Nielson, P. E. *Bioconjugate Chem.* **1991**, *2*, 1.

(5) Bailly, C.; Hénichart, J.-P. *Bioconjugate Chem.* **1991**, *2*, 379.

(6) (a) Zhang, X.; Patel, D. J. *Biochemistry* **1991**, *30*, 4026. (b) Zhang, X.; Patel, D. J. *Biochemistry* **1990**, *29*, 9451. (c) Norman, D.; Live, D.; Sastry, M.; Lipman, R.; Hingerty, B. E.; Tomasz, M.; Broyde, S.; Patel, D. J. *Biochemistry* **1990**, *29*, 2861. (d) Fede, A.; Labhardt, A.; Bannwarth, W.; Leupin, W. *Biochemistry* **1991**, *30*, 11377. (e) Umemoto, K.; Sarma, M. H.; Gupta, G.; Luo, J.; Sarma, R. H. *J. Am. Chem. Soc.* **1990**, *112*, 4539. (f) Boehncke, K.; Nonella, M.; Schulten, K. *Biochemistry* **1991**, *30*, 5465. (g) Embrey, K. J.; Searle, M. S.; Craik, D. J. *J. Chem. Soc., Chem. Commun.* **1991**, 1770. (h) Kumar, S.; Jaseja, M.; Zimmermann, J.; Yadagiri, B.; Pon, R. T.; Sapse, A.-M.; Lown, W. J. *J. Biol. Struct. Dyn.* **1990**, *8*, 99. (i) Pelton, J. G.; Wemmer, D. E. *Proc. Natl. Acad. Sci.* U.S.A. **1989**, *86*, 5723. (j) Pelton, J. G.; Wemmer, D. E. *Biochemistry* **1988**, *27*, 8088. (k) Fagan, P.; Wemmer, D. E. *J. Am. Chem. Soc.* **1992**, *114*, 1080. (l) Keniry, M. A.; Banville, D. L.; Levenson, C.; Shafer, R. H. *FEBS Lett.* **1991**, *289*, 210. (m) Lee, M.; Shea, R. G.; Hartley, J. A.; Kissinger, K.; Pon, R. T.; Vesnaver, G.; Breslauer, K. J.; Dabrowiak, J. C.; Lown, J. W. *J. Am. Chem. Soc.* **1989**, *111*, 345. (n) Boyd, F. L.; Cheatham, S. F.; Ramers, W.; Hill, G. C.; Hurley, L. H. *J. Am. Chem. Soc.* **1990**, *112*, 3279. (o) Lee, M.; Krowicki, K.; Hartley, J. A.; Pon, R. T.; Lown, J. W. *J. Am. Chem. Soc.* **1988**, *110*, 3641. (p) Rao, K. E.; Lown, J. W. *Chem. Res. Toxicol.* **1991**, *4*, 661. (q) Boger, D. L.; Sakya, S. M. *J. Org. Chem.* **1992**, *57*, 1277. (r) Lin, C. H.; Hill, G. C.; Hurley, L. H. *Chem. Res. Toxicol.* **1992**, *5*, 167.

0002-7863/93/1515-7080$04.00/0

Scheme I

a

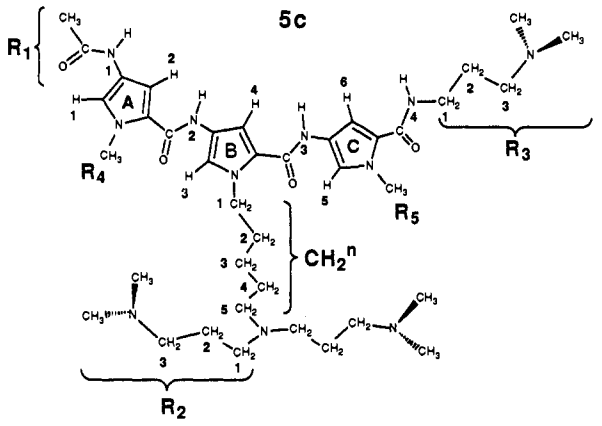

b

5'- C$_1$ G$_2$ C$_3$ A$_4$ A$_5$ A$_6$ T$_7$ T$_8$ T$_9$ G$_{10}$ C$_{11}$ G$_{12}$ -3'

3'- G$_{-1}$ C$_{-2}$ G$_{-3}$ T$_{-4}$ T$_{-5}$ T$_{-6}$ A$_{-7}$ A$_{-8}$A$_{-9}$C$_{-10}$ G$_{-11}$ C$_{-12}$ -5'

Dien-microgonotropen-c (**5c**, Scheme Ia), like the lexitropsins distamycin and netropsin, is a minor groove binder with an affinity for A+T-rich regions.[8] The novel feature of the structure of **5c** is the central polyamino entity, which must reside out of the minor groove. The objective of this study has been to determine the structure of the 1:1 complex of d(CGCAAATTTGCG)$_2$ with **5c** in aqueous solution using nuclear Overhauser effect spectroscopy (NOESY)[9] and restrained molecular modeling (RM).[10] In order to achieve this goal, we have determined the solution structure of the dodecamer alone starting from its crystal structure[11] using RM with NOE-derived distance constraints. The solution structure of the dodecamer was used to initiate the docking and modeling of the binding of **5c** using constraints based on NOEs and on RM calculations with CHARMm parameters.[10]

Results

Previous studies by ^{1}H NMR of distamycin–DNA complexes include the determination of the rate constants for dissociation of 1:1 and 2:1 complexes of distamycin with d(CGCGAATTCGCG)$_2$ and d(CGCAAATTGGC)/d(GCCAATTTGCG), respectively.[6l,12,13] Partial assignments of resonances for d(CGCAAATTTGCG)$_2$ and semiquantitative analysis for the 2:1 complex of distamycin with this dodecamer duplex have been reported.[13] For the correct interpretation of the structural and dynamic data, the complete assignment of the complex NMR spectra is necessary. This has been shown to be possible using 2D ^{1}H NMR spectroscopy (NOESY and ROESY).[14] However, the rules which have been developed for the assignment of DNA ^{1}H resonances must be treated with reasonable flexibility due to the fact that the binding of a ligand may change the conformation of the DNA. For example, the general interaction of the nucleotide base H6 or H8 proton with the H2″ proton of the sugar of the previous nucleotide unit (nH6/8 to (n–1)H2″) may change to interactions involving the H1′ (nH6/8 to (n–1)H1′). [For the notations see Scheme I and Experimental Section.] The main and final task of these kinds of studies is the search for intermolecular NOEs, providing the basis for the structural characterization of the DNA–ligand complexes.[6d]

Under the conditions of these NMR experiments, only the 1:1 **5c** to dodecamer complex was seen. This was shown by the unchanged imino proton region after reaching the 1:1 ratio when we titrated the DNA with **5c** in 9:1 H_2O/D_2O (vida infra). With distamycin, Pelton and Wemmer observed by ^{1}H NMR that the binding of a second molecule to d(CGCAAATTTGCG)$_2$ was slightly more favorable than the binding of the first.[13]

Assignment of the ^{1}H chemical shifts in the uncomplexed dodecamer was made in D_2O solution (10 °C; μ = 1.2). Partial assignment of ^{1}H resonances for d(CGCAAATTTGCG)$_2$ has previously been reported.[13] A more complete assignment of the ^{1}H resonances is shown in Table I (see also Figures 1 and S1–S3).

In the aromatic adenosine region (Figure 1), A$_6$H8 was assigned from T$_7$CH$_3$. The resonance at 8.20 ppm gives strong NOEs in the H2′2″ region at 2.75 and 2.90 ppm, and that of 8.11 ppm gives strong NOEs at 2.67 and 2.9–3.0 ppm (composite peak). A$_6$H8 (8.09 ppm) gives enhancements at 2.55 ppm (A$_6$H2′) and a composite peak at 2.9–3.0 ppm (A$_5$H2″ + A$_6$H2″) overlapped with NOEs of the resonance at 8.11 ppm, which we consider to be A$_4$H8. If we consider the resonance at 8.11 ppm to be A$_5$H8 and that of 8.20 ppm to be A$_4$H8, then the NOE at 8.20/2.75 ppm can be explained as the aromatic H8 to H2′ of the same residue, but the peak at 8.20/2.90 ppm has to be a combination of a relatively strong interaction with (n–1)H2″ and a weak interaction with nH2″ (we previously described the interaction with nH2′ to be at 8.20/2.75 ppm). In either event, the (n–1)-H2″ will dominate the NOE. Since for A$_4$H8 the (n–1)H2″ is C$_3$H2″, which is located at 1.89 ppm, the resonance at 8.20 ppm must be A$_5$H8 (Figure 1). This is consistent with the assignment of A$_6$H2 (7.55 ppm) downfield from A$_4$H2 (7.17 ppm), which in turn is downfield from A$_5$H2 (7.03 ppm) (Table I and ref 13). The H1′ and H3′ resonances were assigned from their H2′2″ neighbors, and the H5′5″ and H4′ (where possible), from H3′ and H1′ resonances, respectively (Figures S3 and S4 and Table I). All of our assignments agree with the partial assignments of the previous work[13] done on the same oligonucleotide, except for A$_4$H8 and A$_5$H8, which have been, in our opinion, reversed in ref 13.

Titration of d(CGCAAATTTGCG)$_2$ with 5c. In order to establish the stoichiometry of binding, the imino (exchangeable) protons were used as minor groove binding markers. By titrating d(CGCAAATTTGCG)$_2$ with **5c** (Figure 2), all three A=T starting imino proton resonances (13.5–14.2 ppm, marked with asterisks) disappear at a 1:1 ratio. No further changes can be detected when further titrating from 1:1 to 2:1 **5c**/DNA mole ratio. The G≡C region (12.6–13.1 ppm) involves only one set of imino resonances, which disappears (at a 1:1 ratio), leading to two distinct up- and downfield-shifted resonances. Upon binding **5c**, broadening occurs in the A=T region.[6e] The broad

(7) (a) Alam, T. M.; Orban, J.; Drobny, G. P. *Biochemistry* **1991**, *30*, 9229. (b) Admiraal, G.; Alink, M.; Altona, C.; Dijt, F. J.; van Garderen, C. J.; de Graaf, R. A. G.; Reedijk, J. *J. Am. Chem. Soc.* **1992**, *114*, 930. (c) Wang, A. H.-J.; Ughetto, G.; Quigley, G. J.; Hakoshima, T.; van der Marel, G. A.; van Boom, J. H.; Rich, A. *Science* **1984**, *225*, 1115. (d) Ughetto, G.; Wang, A. H.-J.; Quigley, G. J.; van der Marel, G. A.; van Boom, J. H.; Rich, A. *Nucleic Acids Res.* **1985**, *13*, 2305. (e) Quigley, G. J.; Ughetto, G.; van der Marel, G. A.; van Boom, J. H.; Wang, A. H.-J.; Rich, A. *Science* **1986**, *232*, 1255. (f) Quintana, J. R.; Lipanov, A. A.; Dickerson, R. E. *Biochemistry* **1991**, *30*, 10294. (g) Coll, M.; Frederick, C. A.; Wang, A. H.-J.; Rich, A. *Proc. Natl. Acad. Sci.* U.S.A. **1987**, *84*, 8385. (h) Kopka, M. L.; Yoon, C.; Goodsell, D.; Pjura, P.; Dickerson, R. E. *Proc. Natl. Acad. Sci.* U.S.A. **1985**, *82*, 1376.

(8) (a) He, G.-X.; Browne, K. A.; Groppe, J. C.; Blaskó, A.; Mei, H.-Y.; Bruice, T. C. *J. Am. Chem. Soc.*, first of three papers in this issue. (b) Browne, K. A.; He, G.-X.; Bruice, T. C. *J. Am. Chem. Soc.*, second of three papers in this issue.

(9) Jeener, J.; Meier, B. H.; Bachmann, P.; Ernst, R. R. *J. Chem. Phys.* **1979**, *71*, 4546.

(10) *QUANTA*, version 3.2.3; Polygen/Molecular Simulations: Waltham, MA, 1991.

(11) Provided by C. A. Frederick prior to actual release (see ref 7g).

(12) Klevit, R. E.; Wemmer, D. E.; Reid, B. R. *Biochemistry* **1986**, *25*, 3296.

(13) Pelton, J. G.; Wemmer, D. E. *J. Am. Chem. Soc.* **1990**, *112*, 1393.

(14) (a) Patel, D. J.; Kozlowski, S. A.; Marky, L. A.; Broka, C.; Rice, J. A.; Itakura, K.; Breslauer, K. J. *Biochemistry* **1982**, *21*, 428. (b) Hare, D. R.; Wemmer, D. E.; Chou, S.-H.; Drobny, G.; Reid, B. R. *J. Mol. Biol.* **1983**, *171*, 319.

Table I. ^{1}H Chemical Shifts for d(CGCAAATTTGCG)$_2$ in D_2O[a]

base	H1′	H2′	H2″	H3′	H4′	H5′	H5″	H6/8	H2/5/CH$_3$
5′-C_1	5.78	1.99	2.42	4.71	4.08	4.08	3.73	7.65	5.92
5′-G_2	5.90	2.66	2.73	4.96	4.34	4.34	4.33	7.94	
5′-C_3	5.44	1.89	2.23	4.94	nd[b]	4.18	4.12	7.32	5.43
5′-A_4	5.91	2.67	2.91	5.06	4.22	4.47	4.23	8.11	7.17
5′-A_5	5.81	2.75	2.89	5.05	4.40	4.48	4.39	8.20	7.03
5′-A_6	6.13	2.55	2.95	5.01	4.25	4.48	4.39	8.09	7.55
5′-T_7	5.93	2.04	2.61	4.91	4.23	4.25	4.18	7.11	1.26
5′-T_8	6.15	2.20	2.65	4.92	nd	4.24	4.15	7.43	1.54
5′-T_9	5.89	2.10	2.50	4.92	4.15	4.25	4.18	7.30	1.67
5′-G_{10}	5.83	2.39	2.70	5.01	nd	4.18	4.12	7.92	
5′-C_{11}	5.79	1.92	2.36	4.87	nd	4.18	4.12	7.36	5.43
5′-G_{12}	6.16	2.39	2.64	4.70	nd	4.18	4.12	7.96	

[a] δ, in ppm, relative to TSP at 25 °C. The DNA concentration was 3.9 mM (duplex) in 10 mM phosphate buffer, pH 7.0, and 10 mM NaCl; H5″ was defined as being the proton closest to the aromatic ring. [b] Not determined.

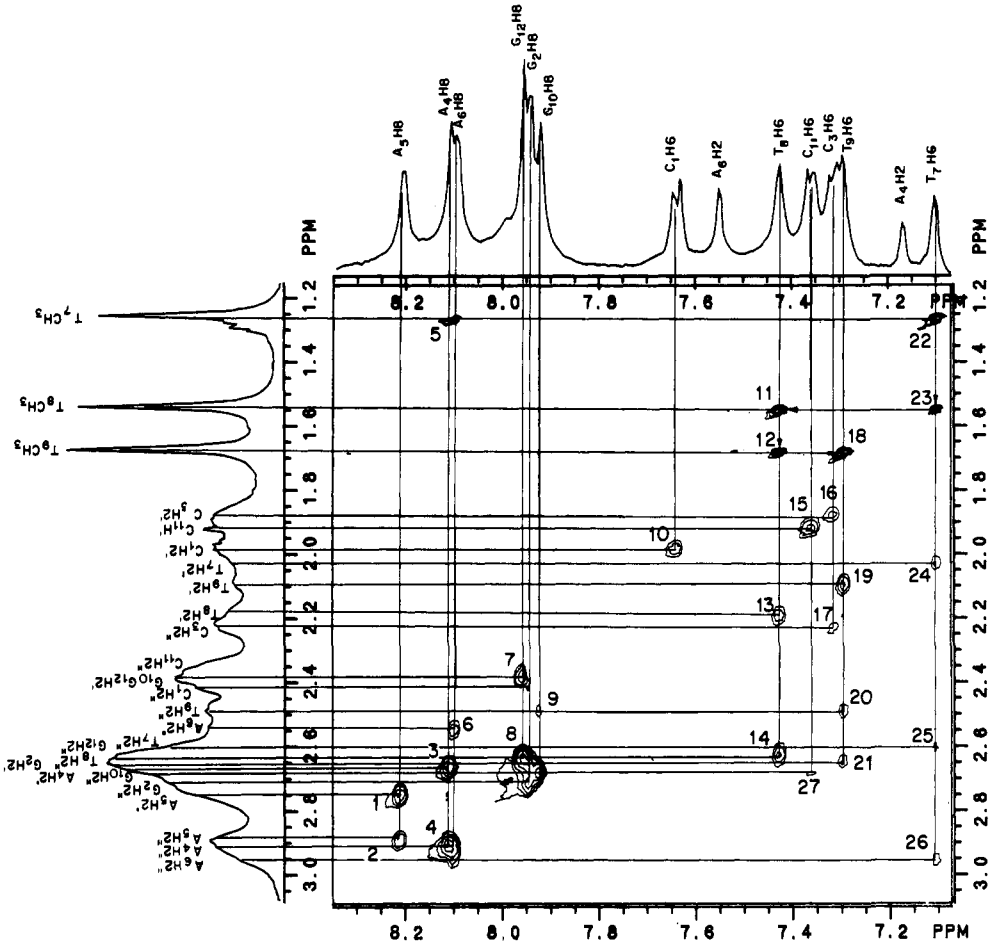

Figure 1. Expansion of the NOESY spectrum in the (7.1–8.3) × (1.2–3.1) ppm region of d(CGCAAATTTGCG)$_2$ at 3.9 mM in 99.96% D_2O containing 10 mM NaCl and 10 mM phosphate buffer, pH 7.0 at 25 °C (τ_m = 300 ms): (1) A_5H8–A_5H2'; (2) A_5H8–A_5H2''; (3) A_4H8–A_4H2'; (4) A_4H8–A_4H2'', A_6H8–A_5H2''; A_6H8–A_6H2''; (5) A_6H8–T_7CH_3; (6) A_6H8–A_6H2'; (7) $G_{12}H8$–$C_{12}H2'$, G_2H8–C_1H2''; (8) $G_2G_{10}G_{12}H8$–$G_2G_{10}G_{12}H2''$, G_2H8–G_2-H2′; (9) $G_{10}H8$–T_9H2''; (10) C_1H6–C_1H2'; (11) T_8H6–T_8CH_3; (12) T_8H6–T_9CH_3; (13) T_8H6–T_8H2'; (14) T_8H6–T_8H2''; (15) $C_{11}H6$–C_1H2'; (16) C_3H6–C_3H2'; (17) C_3H6–C_3H2''; (18) T_9H6–T_9CH_3; (19) T_9H6–T_9H2'; (20) T_9H6–T_9H2''; (21) T_9H6–T_8H2''; (22) T_7H6–T_7CH_3; (23) T_7H6–T_8CH_3; (24) T_7H6–T_7H2'; (25) T_7H6–T_7H2''; (26) T_7H6–A_6H2''; (27) $C_{11}H6$–$G_{10}H2''$.

resonances disappear in the t_1 noise under the experimental conditions (Figure 2), but they can be seen at higher concentrations (Figure S5).

Assignment of ^{1}H Chemical Shifts of d(CGCAAATTTGCG)$_2$ in the 1:1 Complex with 5c. Two sets of Watson–Crick G≡C and A=T resonances at around 13 and 14 ppm, respectively, are indicative of an asymmetric binding of the ligand to the DNA molecule. Deconvolution of these overlapped peaks (Figure S5) shows that the broadening is different along the A=T pairing ($\nu_{1/2}$ = 40–170 Hz), while on the G≡C the broadening does not change significantly ($\nu_{1/2}$ = 40 Hz) except for one peak which has $\nu_{1/2}$ = 90 Hz. Two out of six A=T imino resonances have line widths around 40 Hz, one has a line width of 50 Hz, and the remaining three have line widths between 90 and 170 Hz. This indicates an involvement of three or four A=T and one G≡C base pairs in the binding.

Expansion of the NOESY spectrum of the aromatic to aliphatic region (Figure 3) shows the general pattern of pair enhancements, H6/8–H2′2″, H1′–H2′2″, H3′–H5′5″, H3′–H2′2″, used for the assignment of sugar proton resonances (Table II). We use the convention that the (+) strand is the binding-site side and the (–) strand is the complementary DNA strand. The resonances of $T_7T_{-6}CH_3$ are good starting markers, as found in the case of free DNA. The interpretation of the NOEs is rather difficult, since two sets of resonances can be seen in almost all cases, representing an asymmetric type of binding of the ligand to the DNA molecule.

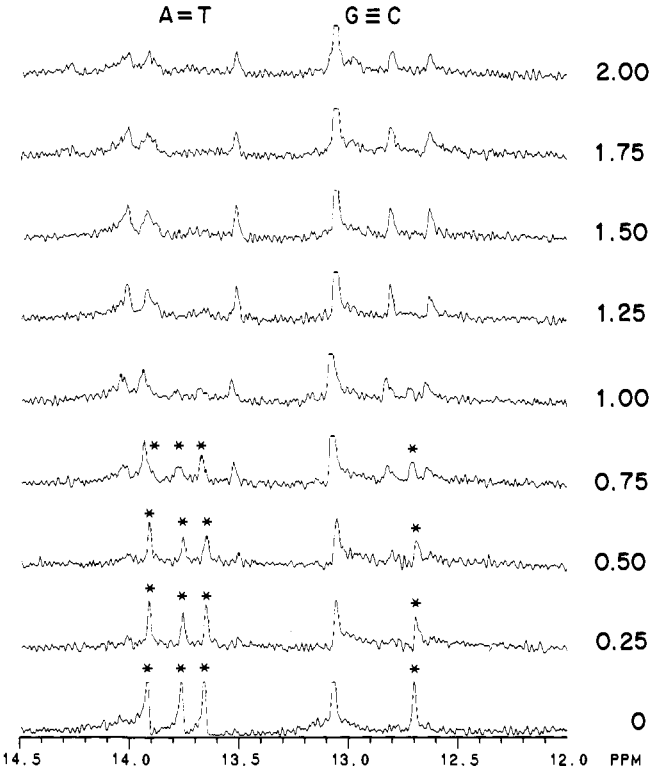

Figure 2. Titration with **5c** of a 1.8×10^{-4} M solution of d(CGCAAATTTGCG)$_2$ containing 10 mM NaCl and 10 mM phosphate buffer, pH 7.0, in 9:1 H_2O/D_2O at 21 °C. The **5c**/DNA mole ratios are shown along the side of the spectra. At a 1:1 ratio, no spectral changes (followed by the resonances marked with asterisks) occur when titrating up to a 2:1 ratio.

The aromatic resonances were assigned using the known resonances of cytidine H6/5 (DQF-COSY, not shown) which give strong intraresidual NOEs (Figure 4) and thymidine H6 (from their corresponding methyl neighbors). We also used the proven fact that **5c** is a minor groove binder into the A+T-rich region.[2a,8] The guanosine H8 resonances (7.9–8.0 ppm) were used to define the T_9H6, G_{12}H1′, and T_{-4}H1′ resonances (Figure 4). The adenosine H8 resonances were assigned using the interactions between two adjacent $A_{n-1}A_n$H8 protons (8.16 and 8.27 ppm) and the information coming from the free DNA data. By comparing the NOE buildups for the free and ligated DNA (Figures 1 and 3) in the aromatic to aliphatic region, we note weaker interactions (small NOEs) of the A_6H8 with A_6H2′ and A_5H2″ than those in the case of A_4H8 and A_5H8 for free DNA and no interactions (no NOEs) for the complexed DNA. No T_7CH_3 to A_6H8 or C_3H2″/H1′ to A_4H8 interactions in the 1:1 complex were seen. A_6H8 gives NOE in the H1′ region, somewhat downfield from that in free DNA; this resonance belongs to A_6-H1′, an important marker for the intermolecular interactions.

The highly overlapped H5′5″ peaks were resolved by using the relation between H3′ and H2′2″. The straight line coming from H3′ and passing through H2′2″ (Figure 3) intersects the overlapped NOE peaks of the H5′5″ region, giving H5′ and H5″ resonances to within a reasonable approximation. In the estimation of H5′ and H5″, the shape of these complex NOEs and the number of contour levels were taken into account.

Assignment of 5c resonances in $CDCl_3$ has been reported[8] and was used as a lead for the assignment in D_2O. By comparing the 5.9–6.4 ppm region for distamycin[13] and **5c** (Figure 4) when bound to d(CGCAAATTTGCG)$_2$, we recognize the H2, H4, and H6 pyrrole resonances of **5c** (Scheme Ia) as being strongly upfield-shifted, indicative of the minor groove binding. They give NOEs with adenosine A_{-7}H2 aromatic protons of the (-) strand and with the sugar A_6T_7H1′, T_7H1′, and T_9H1′ protons, respectively. H1, H3, and H5 resonances were assigned using

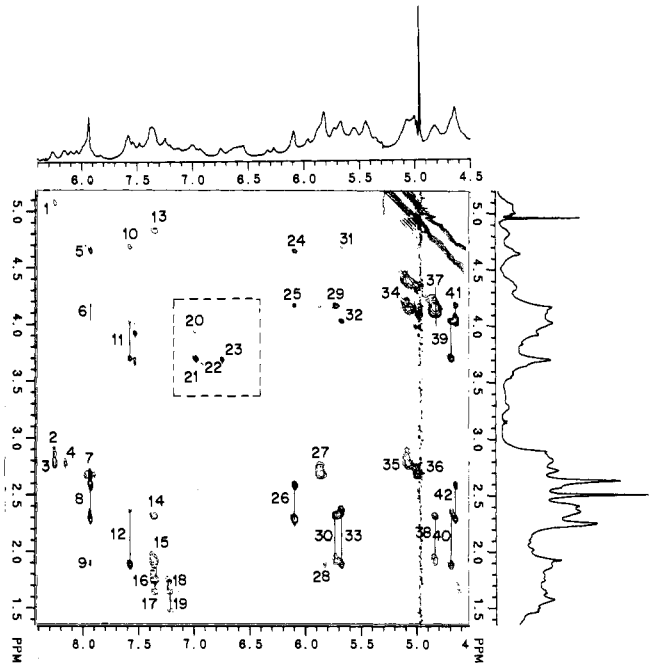

Figure 3. Expansion of the NOESY spectrum in the (1.4–5.2) × (4.5–8.4) ppm region of the 1:1 complex of d(CGCAAATTTGCG)$_2$ at 3.9 mM with **5c** in 99.96% D_2O containing 10 mM NaCl and 10 mM phosphate buffer, pH 7.0 at 10 °C (τ_m = 200 ms): (1) A_5H8–A_5H3′; (2) A_5H8–A_4H2″; (3) A_5A_{-7}H8–A_5A_{-7}H2′; (4) A_4H8–A_4H2′; (5) G_{12}-H8–G_{12}H3′; (6) $G_{10}G_{12}$H8–$G_{10}G_{12}$H5′5″; (7) G_2H8–G_2H2′; (8) $G_{10}G_{12}$-H8–$G_{10}G_{12}$H2′2″; (9) G_{12}H8–C_{11}H2″; (10) C_1H6–C_1H3′; (11) C_1H6–C_1H5′5″; (12) C_1H6–C_1H2′2″; (13) T_8T_9H6–T_8T_9H3′; (14) T_8T_9H6–T_8T_9H2″; (15) T_8T_9H6–T_8T_9H2′, C_3C_{11}H6–C_3C_{11}H2′; (16) T_9CH_3–T_8T_9H6; (17) T_8CH_3–T_8H6; (18) $T_8T_{-5}CH_3$–T_7T_{-6}H6; (19) $T_7T_{-6}CH_3$–T_7T_{-6}H6; (20) H1–A_6H5″; (21) H1–CH_3^{R4}; (22) H5–CH_3^{R5}; (23) H3–CH_3^{R4}; (24) G_{12}H1′–C_{11}H3′; (25) G_{12}H1′–G_{12}H4′; (26) G_{12}-H1′–G_{12}H2′H2″; (27) G_2H1′–G_2H2′H2″; (28) C_1H5–C_1H2′; (29) T_{-4}H1′–T_{-4}H4′; (30) T_{-4}H1′–T_{-4}H2′2″, C_1H1′–G_2H3′; (32) C_1H1′–C_1H4′; (33) C_1H1′–C_1H2′2″; (34) $A_4A_5A_6$H3′–$A_4A_5A_6$H5′5″, G_2H3′–G_2H5′5″; (35) $A_4A_5A_6$H3′–$A_4A_5A_6$H2′2″; (36) G_2H3′–G_2H2′2″; (37) $T_7T_8T_9$H3′–$T_7T_8T_9$H5′5″; (38) $T_7H_8T_9$H3′–$T_7T_8T_9$H2′2″; (39) $C_1C_3C_{11}$-H3′–$C_1C_3C_{11}$H5′5″; (40) $C_1C_3C_{11}$H3′–$C_1C_3C_{11}$H2′2″; (41) $G_{10}G_{12}$H3′–$G_{10}G_{12}$H5′5″; (42) $G_{10}G_{12}$H3′–$G_{10}G_{12}$H2′2″.

their interaction with the DNA molecule (*vide infra*). New interactions can be seen in the (6.7–7.1, 3.6–3.8) ppm area (Figure 3, box) which belong to the intramolecular interactions of the H1, H3, and H5 pyrrole protons of **5c** with their neighboring protons [CH_3^{R5}, CH_3^{R4}, and CH_2^n(1)] (see Scheme I). The methylene resonances of **5c** were assigned from the DQF-COSY spectrum of the 1:1 complex (10 °C) (Figure S6 and Table S1). The aromatic region was studied both in D_2O and in H_2O. In changing from D_2O to H_2O solvent, slow exchange of the amide protons (ca. 8.4 ppm) was observed. The reverse process (H_2O to D_2O) confirmed this observation.

Intracomplex Interactions of Dodecamer and 5c. A good starting marker for the intracomplex interactions is A_6H1′, which leads to a cascade type of resonance assignments (Figure 4) as follows: A_6H1′ gives NOE with H2, H2 with T_7H1′, T_7H1′ with H4, H4 with A_{-7}H2, A_{-7}H2 with H6, and H6 with T_9H1′; T_7H1′ gives NOE with H3, and H3 with T_8H1′. The positions of H1, H3, and H5 were confirmed by their interactions with the pyrrole methyl protons R4 and R5, which do not markedly change their positions as the complex is formed (Table S1).

NOE enhancements were found between $CH_2^{R2}(2)/CH_2^{R2}(3)$ and T_8T_9H2′ protons, CH_3^{R1} and A_6H2″, CH_3^{R4} and A_6H5″, CH_3^{R5} and T_9H5″, as well as between $CH_2^{R2}(3)$ and T_8T_9H5′ (Figures 5 and S7). The interaction between the $CH_2^{R2}(2)$ and T_8T_9H2′ protons suggests that the two (dimethylamino)propyl legs of the dien ligand align along the phosphate backbone parallel

Table II. ^{1}H Chemical Shifts for d(CGCAAATTTGCG)$_2$ in the 1:1 Complex with **5c** in D_2O[a]

base	H1′	H2′	H2″	H3′	H4′	H5′	H5″	H6/8	H2/5/CH$_3$
(+) strand									
5′-C_1	5.58	1.90	2.33	4.67	4.03	4.02	3.70	7.58	5.83
5′-G_2	5.89	2.68	2.73	4.69	nd[b]	4.30	4.32	7.98	
5′-C_3	5.43	1.90	2.33	4.64	nd	4.10	4.02	7.38	5.43
5′-A_4	6.10	2.80	2.88	5.02	nd	4.40	4.14	8.16	7.15
5′-A_5	6.10	2.83	2.89	5.08	nd	4.44	4.20	8.27	7.83
5′-A_6	6.54	2.77	2.85	5.00	nd	4.36	4.00	8.10	nd
5′-T_7	6.57	1.90	2.30	4.80	nd	4.17	4.14	7.25	1.50
5′-T_8	7.02	1.90	2.30	4.86	nd	4.16	4.12	7.43	1.65
5′-T_9	6.62	1.90	2.30	4.83	4.16	4.17	4.05	7.35	1.75
5′-G_{10}	5.60	2.25	2.57	4.64	nd	4.16	4.05	7.94	
5′-C_{11}	5.55	1.90	2.33	4.64	nd	4.02	3.70	7.38	5.43
5′-G_{12}	6.10	2.25	2.57	4.64	4.16	4.16	4.05	7.94	
(−) strand									
5′-C_{-12}	5.68	1.90	2.33	4.67	4.03	4.02	3.70	7.58	5.83
5′-G_{-11}	5.89	2.68	2.73	4.69	nd	4.30	4.32	7.98	
5′-C_{-10}	5.36	1.90	2.33	4.64	nd	4.10	4.02	7.38	5.43
5′-A_{-9}	6.10	2.80	2.88	5.02	nd	4.40	4.14	8.16	nd
5′-A_{-8}	6.10	2.83	2.89	5.08	nd	4.44	4.20	8.27	8.26
5′-A_{-7}	7.25	2.77	2.85	5.00	nd	4.36	4.00	8.10	8.06
5′-T_{-6}	7.07	1.90	2.30	4.80	nd	4.17	4.14	7.47	1.48
5′-T_{-5}	6.93	1.90	2.30	4.86	nd	4.16	4.12	7.58	1.63
5′-T_{-4}	5.72	1.90	2.30	4.83	4.16	4.17	4.05	7.55	1.78
5′-G_{-3}	5.60	2.25	2.57	4.64	nd	4.16	4.05	7.94	
5′-C_{-2}	5.55	1.90	2.33	4.64	nd	4.02	3.70	7.38	5.43
5′-G_{-1}	6.10	2.25	2.57	4.64	4.16	4.16	4.05	7.94	

[a] δ in ppm relative to TSP at 10 °C (concentrations as in Table I). The Watson–Crick imino protons (recorded in H_2O) are in the range A=T 13.5–14.2 and G≡C 12.6–13.1 ppm. [b] Not determined.

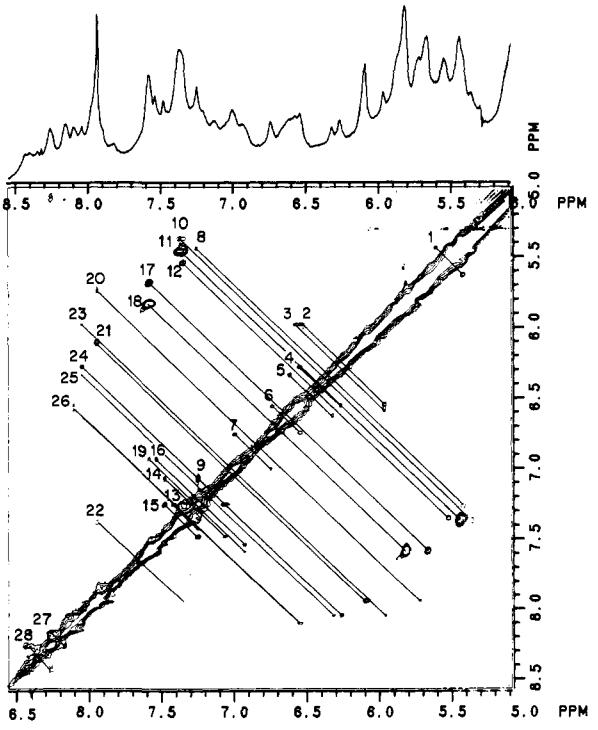

Figure 4. Expansion of the NOESY spectrum in the (5.0–8.5) × (5.0–8.5) ppm region of the 1:1 complex of d(CGCAAATTTGCG)$_2$ at 3.9 mM with **5c** in 99.96% D_2O containing 10 mM NaCl and 10 mM phosphate buffer, pH 7.0 at 10 °C (τ_m = 200 ms): (1) G_{10}H1′–C_{11}H5; (2) H2–A_6H1′; (3) H2–T_7H1′; (4) H4–T_7H1′; (5) H6–T_9H1′; (6) H3–T_7H1′; (7) H3–T_8H1′; (8) C_3H6–C_3H1′; (9) A_{-7}H1′–T_{-6}H1′; (10) C_{-10}H1′–C_3H1′; (11) C_3C_{11}H6–C_3C_{11}H5; (12) C_{11}H6–C_{11}H1′; (13) T_7-H6–T_8H6; (14) T_{-6}H1′–T_{-6}H6; (15) A_{-7}H1′–T_{-6}H6; (16) T_{-5}H1′–T_{-6}H6; (17) C_1H6–C_1H1′; (18) C_1H6–C_1H5; (19) T_{-8}H6–T_{-5}H1′; (20) T_{-4}H1′–G_{-3}H8; (21) G_{12}H1′–G_{12}H8; (22) G_{10}H8–T_9H6; (23) H2–A_{-7}H2; (24) H4–A_{-7}H2; (25) H6–A_{-7}H2; (26) A_6H1′–A_6H8; (27) A_5H8–A_4-H8; (28) NH(3)–A_{-8}H2.

to the tripyrrole peptide residue such that the CH_2^{R2}(2) protons of one leg are close to the sugar T_8H2′ and the CH_2^{R2}(2) protons of the other leg are near the T_9H2′ proton. The possibility of the

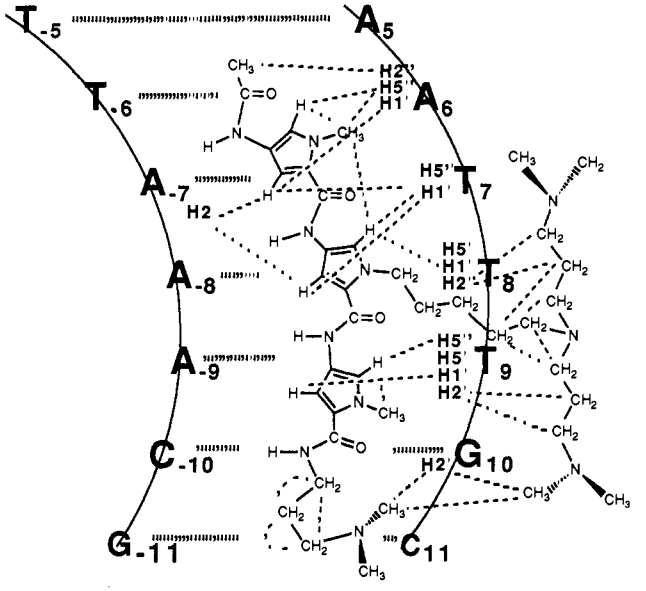

Figure 5. Schematic representation of the intracomplex interactions (NOE signals represented by broken lines) in the 1:1 complex of d(CGCAAATTTGCG)$_2$ at 3.9 mM with **5c** in 99.96% D_2O containing 10 mM NaCl and 10 mM phosphate buffer, pH 7.0 at 25 °C in D_2O.

T_8T_9H2′ interactions with the same CH_2^{R2}(2) protons was ruled out because of steric and electronic effects. A 2:1 symmetrical binding mode was ruled out by the two sets of imino protons, and the 2:1 asymmetric mode was ruled out by the existence of a single set of ligand resonances. Both types of 2:1 binding modes were further ruled out by the NMR titration experiment (Figure 2). The interaction between the CH_2^{R2}(3) and T_8T_9H2′ protons is consistent with the earlier assumption that the dien ligand is aligning along the phosphate backbone. T_7H2′ resonates in the same place as T_8T_9H2′. However, a less likely contact of the CH_2^{R2}(2) and CH_2^{R2}(3) with T_7H2′ can occur, since G_{10}H2′ interactions with CH_3^{R2} protons were detected (see following) and, therefore, T_7H2′ cannot be reached by the R2 methylenes.

Expansion of the (2.1–3.1) × (2.0–3.0) ppm region of the NOESY spectrum (Figure 6) reveals proximities between CH_3^{R3}/CH_3^{R2} and G_{10}H2′ (major groove pointer), as well as between the

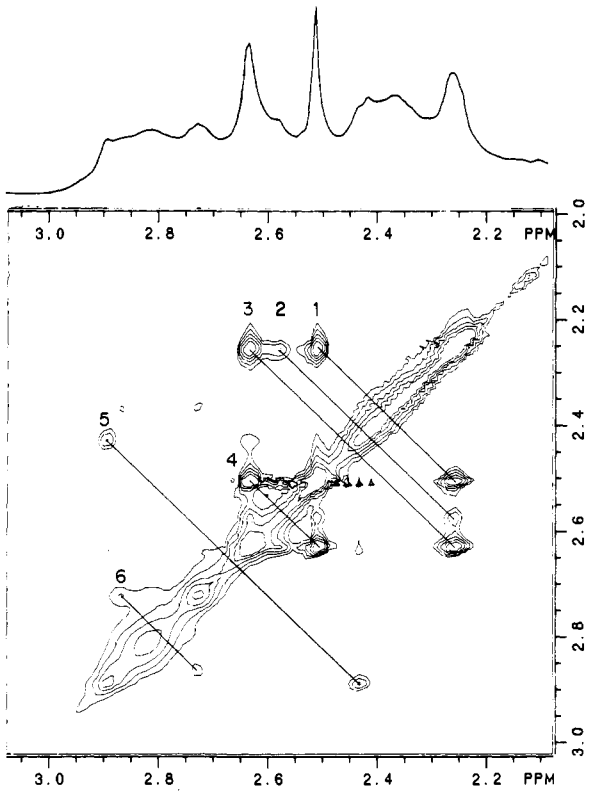

Figure 6. Expansion of the NOESY spectrum in the (2.1–3.1) × (2.0 –3.0) ppm region of the 1:1 complex of d(CGCAAATTTGCG)$_2$ at 3.9 mM with **5c** in 99.96% D_2O containing 10 mM NaCl and 10 mM phosphate buffer, pH 7.0 at 10 °C (τ_m = 200 ms): (1) CH_3^{R2}–$G_{10}H2'$; (2) $G_{10}H2''$–$G_{10}H2'$; (3) CH_3^{R3}–$G_{10}H2'$; (4) CH_3^{R2}–CH_3^{R3}; (5) $CH_2^{n}(5)$–$CH_2^{R2}(1)$; (6) $CH_2^{R3}(1)$–$CH_2^{R3}(3)$.

CH_3^{R3} and CH_3^{R2} protons. This provides evidence for the alignment of the (dimethylamino)propyl leg with the (dimethylamino)propyl tail and the major groove position of R2. Though $G_{10}H2'$ resonates in the same place as $G_{12}H2'$, NOEs cannot occur with $G_{12}H2'$, considering the size of the ligand and its isohelical alignment into the A+T-rich minor groove. Other ligand intramolecular interactions confirm our assignments (Figure 5 and Table II). We could not see and/or separate interactions of CH_3^{R1} with the A_6H1' protons due to the congestion in this region. The reason we assigned the NOE at 1.93/2.35 ppm to the CH_3^{R1}–A_6H2'' proton interaction (Figure S7) was that the thymidine H2′ protons, resonating in the same region as the CH_3^{R1} protons, cannot interact with the adenosine H2′/2″ or with the $CH_2^{R3}(1)$ protons. Since the antiparallel 2:1 mode of binding was ruled out, it is not possible to have interactions between CH_3^{R1} and $CH_2^{R3}(1)$. Close to the diagonal in the NOESY spectrum (Figure S7), interactions can be seen between the pyrrole methyl groups (R4 and R5) and the methylene protons (H5′5″) of the phosphate backbone as well as some DNA intramolecular and ligand intramolecular interactions. A survey of the sequential NOEs for the DNA-selected protons in the free and ligated DNA is shown in Table III.

As a result of the minor groove binding, induced chemical shift differences can be seen (Figures 7 and 8 and Table S1). This is primarily due to the ring current effect from both the DNA and the tripyrrole peptide which extends beyond the binding site. The differences are greater for the H1′ protons (minor groove pointers) than for any other selected protons (Figure 7). They increase in the order H5′ < H5″ ≅ H6/8 < H2′ ≅ H2″ < H1′. As will be seen, the strong deshielding of the H1′ protons is consistent with the restrained molecular modeling structural calculations. Since the pyrroles' H2 and H4 are buried in the minor groove, they are shielded to a greater extent than H1, H3, and H5, which are oriented outward from the groove. The methyl R1 protons are

Table III. Survey of the Sequential NOEs for (a) d(CGCAAATTTGCG)$_2$ and (b) the 1:1 Complex of d(CGCAAATTTGCG)$_2$ with **5c**

a. (+) strand	C$_1$	G$_2$	C$_3$	A$_4$	A$_5$	A$_6$	T$_7$	T$_8$	T$_9$	G$_{10}$	C$_{11}$	G$_{12}$
H6/8 - CH_3						o	o	o	o			
H6/8 - H1'		o	o				o	o	o			
H6/8 - H2''		o	o		o	o	o	o	o	o	o	o
CH_3 - CH_3							o	o				
H6 - H6						o	o	o	o			

b. (+) strand:	C$_1$	G$_2$	C$_3$	A$_4$	A$_5$	A$_6$	T$_7$	T$_8$	T$_9$	G$_{10}$	C$_{11}$	G$_{12}$
H6/8 - CH_3/H5/6/8				o	o		o	o	o	o	o	
H6/8/5 - H1'										o	o	
H6/8 - H2''			o	o	o		o	o	o		o	o
H1' - H3'		o	o								o	o

b. (-) strand:	C$_{-12}$	G$_{-11}$	C$_{-10}$	A$_{-9}$	A$_{-8}$	A$_{-7}$	T$_{-6}$	T$_{-5}$	T$_{-4}$	G$_{-3}$	C$_{-2}$	G$_{-1}$
H6/8 - CH_3/H5/6/8				o	o		o	o	o	o		
H6/8 - H1'							o	o	o	o		
H6/8 - H2''			o	o	o						o	o
H1' - H3'		o	o								o	o
H1' - H1'							o	o				

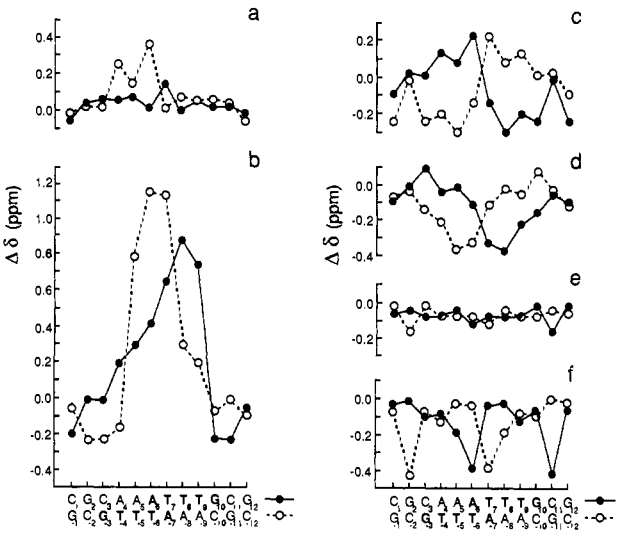

Figure 7. Induced chemical shift differences between the 1:1 complex of d(CGCAAATTTGCG)$_2$ with **5c** and the free DNA vs the DNA sequence for the selected DNA protons: (a) H6/8; (b) H1′; (c) H2′; (d) H2″; (e) H5′; (f) H5″. $\Delta\delta = \delta_{complex} - \delta_{free\ DNA}$.

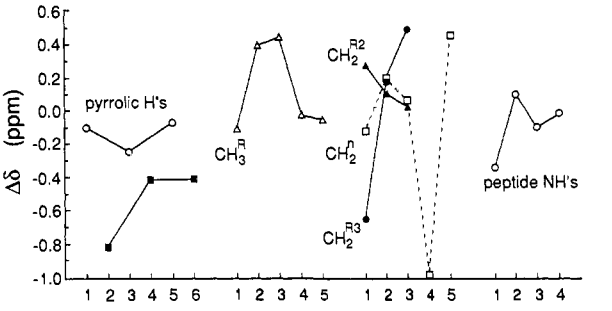

Figure 8. Induced chemical shift differences between the 1:1 complex of d(CGCAAATTTGCG)$_2$ with **5c** and the free DNA vs the specified attached atoms (see Scheme I) for the selected **5c** protons.

slightly shielded, and R2 and R3 are strongly deshielded, whereas the chemical shifts for R4 and R5 do not significantly change. The CH_2^n methylene protons reflect a conformation in which the $(CH_2)_5$ chain extends from the pyrrole nitrogen up to the

Table IV. Experimental (NOESY) and Refined (Molecular Modeling) Distances for d(CGCAAATTTGCG)$_2$ in D_2O[a]

proton		H1′	H2′	H2″	H3′	CH_3/H_5 or H6/8*
C_1	H6	3.7 (3.7)	2.9 (2.9)			
	H5″				3.3 (3.2)	
G_2	H8			3.7[b] (3.7)		
	H5″				3.1 (3.1)	
C_3	H6		3.1 (2.9)	3.5 (3.7)		2.45[c]
	H5″				3.2 (3.2)	
A_4	H8	3.7 (3.7)	2.6 (2.6)			
	H5″				3.2 (3.0)	
	H5′				3.8 (3.8)	
A_5	H8		2.8 (2.8)	2.9 (3.6)		
	H5″				3.2 (2.8)	
A_6	H8		3.7 (3.3)			
	H5″				3.8 (3.8)	
T_7	H6		3.4 (2.7)	3.7 (3.7)		
				3.6[b] (3.5)		
	H5″				3.7 (3.2)	
	CH_3	3.8[b] (3.8)	3.6[b] (3.6)			3.4[b]* (3.4)
T_8	H6		3.6 (3.3)	2.8 (3.1)		
	H5″				3.0 (2.9)	
	CH_3		4.0[b] (3.8)	3.8[b] (3.8)		4.0[b] (4.0)
						3.2[b]* (3.2)
T_9	H6		2.8 (2.3)	3.3 (3.6)		
				3.6[b] (3.5)		
	H5″				3.0 (3.0)	
	CH_3		3.7[b] (3.7)	4.0[b] (3.0)		2.9[b] (2.9)
						2.9[b]* (3.1)
G_{10}	H8			3.8[b] (3.7)		
	H5″				3.3 (3.2)	
C_{11}	H6		2.7 (2.7)	3.8 (3.9)		
				3.8[b] (3.8)		
	H5″				3.4 (3.0)	
G_{12}	H8		3.0 (3.0)			
	H5″				3.5 (3.2)	

[a] In Å, with the same residue. Refined values are in parentheses. [b] Distances with the (n − 1) residue. [c] C_3H5–C_3H6 taken as known separation. Distances marked with asterisks belong to the protons marked with asterisks.

phosphodiester ridge. This connects to the N[$CH_2CH_2CH_2$N-$(CH_3)_2$]$_2$ which resides along the phosphodiester ridge. Thus, CH_2^n(1) and (4) are more shielded than CH_2^n(2) and (3). The shielding of the methylene protons in the 3-(dimethylamino)-propyl moiety decreases from CH_2^{R3}(1) to CH_2^{R3}(2) and changes to a deshielding of CH_2^{R3}(3). A survey of the NOESY interactions in the DNA complex with **5c** is shown in Figure 5.

Distance Calculations and Restrained Molecular Modeling Refinements. For the dodecamer d(CGCAAATTTGCG)$_2$, 78 NOE interactions were seen, from which 66 distances (where the NOEs were not overlapped) were calculated (Experimental Section and Table IV) and 47 were used for the two equivalent strands as distance constraints in the RM calculations using CHARMm force field parameters.[10] C. A. Frederick's crystal structure coordinates of the DNA oligomer d(CGCAAATTTGCG)$_2$ were used[11] as the starting structure. Most of the refined distances agree with the NOE calculated data, and all distances were within 1.0 Å of the calculated values. Violations of a 0.5-Å distance range (upper and lower limit) were found for only four of the H2′2″ proton constraints (A_5H2″–A_5H8; T_7H2′–T_7H6; T_8H2″–T_9CH_3; and T_9H2′–T_9H6) where spin diffusion has a significant contribution.[6j,15] The H2′2″ interactions with the H6/8 protons of the same residue exhibit a deviation of up to 0.9 Å from the experimental and calculated values, which is as expected for the H2′2″ protons at a 300 ms mixing time.[6j,15] Root-mean-square (RMS) deviations to the starting X-ray crystal structure were calculated for the minimized solution structure containing NOE-derived constraints as well as the X-ray crystal structure when minimized without constraints. The RMS deviations were found to be 1.58 for the constrained solution structure and 1.02 for the nonconstrained crystal structure. We define the solution structures as being the most probable (NOE-calculated constraints with CHARMm minimization) structures which fit the NOE-derived distances. In the solution dodecamer, the minor groove narrows considerably between the T_{-5}–T_9 and T_{-4}–T_8 phosphates (from 3 to 1 Å, respectively) relative to the starting crystal structure while CHARMm minimization of the starting crystal structure only narrowed the minor groove by 0.3 to 1 Å in the same region. In solution, when complexed with **5c** or free, d(CGCAAATTTGCG)$_2$ has changed helical parameters compared to the crystal structure. The angle of the bend in the helical axis of the constrained solution dodecamer (21.4°) is roughly 2–3 times greater than those of the crystal[11] and minimized crystal structures (10.8° and 7.5°, respectively) (Table V; Experimental Section). Further comparisons between our proposed solution structure of the free DNA and the starting structure crystallographic data of Frederick are shown in Table V.

For the 1:1 complex of the dodecamer and **5c**, 105 intramolecular interactions were found for both NMR-nonequivalent strands. Of these, 28 were used previously in determining the dodecamer solution structure. These 28 intramolecular interactions represent the only well-separated cross peaks (Table VI). Twenty-one ligand–DNA and ligand–ligand interactions were detected, and all were used for docking (Figure 5). The same minimization procedure used in the case of the uncomplexed DNA (Experimental Section) was employed to obtain the most probable solution structure of the 1:1 complex of **5c** with d(CGCAAATTTGCG)$_2$ (Figures 9b,c). Deviations of 0.7–1 Å between the calculated and measured values were found only in the cases of H2–A_6H1′, CH_3^{R1}–A_6H2″, CH_2^{R2}(3)–T_7T_9H2″, and CH_2^n(4)–CH_2^{R2}(2), where spin diffusion dominates the NOE. Therefore, we allowed larger limits as distance constraints (upper and lower) in those instances. Only one contact (T_{-5}H1′–T_{-5}H6) had a deviation of >1 Å between the calculated and measured values. The ROESY spectrum (Figure S8) shows that most of the H2′/H2″ protons give ROESY peaks without involving their H2″/H2′ brothers.

In the most favored solution structure of the DNA:**5c** complex (NOE-derived constraints with CHARMm minimization), pyrrole rings A and B are almost coplanar whereas B and C are rotated 68° from coplanarity (Scheme II). Another structure in which the pyrrole rings are essentially all coplanar is less favored energy-wise. AM1 calculations on rings B+C (Scheme II) as in **5c** alone establish that a 2.5 kcal/mol input of energy (equivalent to a good hydrogen bond) is all that is required to change the dihedral defined by ψ_2 in Scheme III from 11.1°, as found in the crystal structures of d(CGCAAATTTGCG)$_2$ complexed with distamycin, to the 68.4° found in the most favored solution structure of the d(CGCAAATTTGCG)$_2$:**5c** complex (note that this value is not for the rotational barrier for ψ_2 from 0° to 180°). Comparison of the solution structures of the dodecamer and dodecamer:**5c** complex shows that the minor groove widens considerably between the T_{-5}–T_9 and T_{-4}–T_8 phosphates (from 3 and 2 Å, respectively) upon complexation of **5c**. The minor groove width actually decreases slightly in the region between T_{-6} and G_{10} upon dodecamer complexation of **5c**. The angle of the bend in the helical axis of the solution structure of the dodecamer complexed with **5c** (17.2°) is considerably greater than the same angle for the crystal structure of the dodecamer alone[11] (10.8°) and is nearly twice that found with the minimized crystal structure plus **5c** (9.8°) (Table V; Experimental Section). Additional helical parameters of the most probable solution structures of **5c** complexed to d(CGCAAATTTGCG)$_2$ are compared with the crystal and NMR-derived structures solved by others of the same dodecamer complexed with distamycin (Table V).

(15) Withka, J. M.; Swaminathan, S.; Srinivasan, J.; Beveridge, D. L.; Bolton, P. H. *Science* **1992**, *225*, 597.

Table V. Comparison of Helical Parameters[a] for NOE-Refined, CHARMm-Minimized, and Some Crystal Structures of d(CGCAAATTTGCG)$_2$ with and without Added Ligands

no.	structure	unit height (Å/repeat)	helical rise (bp/repeat)	axial rise (Å/bp)	turn angle (deg/bp)	helical bend (deg)
1	NOE-refined solution dodecamer	33.86	9.92	3.41	36.28	21.4
2	Frederick's crystal dodecamer[11]	32.69	9.91	3.30	36.34	10.8
3	CHARMm minimization of no. 2[b]	33.17	9.85	3.37	36.55	7.5
4	NOE-refined solution complex of dodecamer with **5c**	34.49	10.13	3.40	35.55	17.2
5	NOE-refined solution complex (ψ_2 constrained to 11.1°)	34.70	10.07	3.45	35.75	20.1
6	CHARMm-minimized complex of no. 3 with **5c**[b]	33.13	9.83	3.37	36.60	9.8
7	Rich's 1:1 distamycin to dodecamer crystal complex[c,7g]	32.50	9.85	3.30	36.54	13.9
8	Wemmer's 2:1 distamycin to dodecamer NMR-refined complex[d,13]	32.51	9.74	3.34	36.98	11.3

[a] Helical parameters are described in the Experimental section. [b] Theoretical structures. [c] Structure from Brookhaven's Protein Data Bank File pdb2dnd.ent. [d] Structure generously provided by D. E. Wemmer.

Table VI. Experimental (NOESY) and Refined (Molecular Modeling) Distances for the 1:1 Complex of d(CGCAAATTTGCG)$_2$ with **5c** in D_2O[a]

a. Distances Involving Only d(CGCAAATTTGCG)$_2$ Protons

	H1′	H2′H3′*	H2″	H5′H5″*	H6/8	CH_3/H5
C_1H6	3.2 (3.4)	3.0 (2.9)	3.8 (4.0)			
C_3H6	3.9 (3.8)					
A_4H8		3.6 (3.3)				
A_5H8		4.1* (4.1)	2.8[b] (2.8)			
A_6H8	4.1 (4.0)					
T_7H6						3.6[c] (3.6)
T_8H6		3.4* (3.4)			5.2[b] (5.2)	3.3[c] (3.3)
T_8CH_3						3.6[b] (3.6)
T_9H6		3.4* (3.4)				
T_9CH_3						3.3[b] (3.3)
G_{10}H8						3.8[c] (3.8)
C_{11}H6	3.8 (3.8)					
	3.8[b] (3.7)					
G_{12}H8	3.5 (3.7)	3.1* (3.1)	3.9[b] (3.8)			
G_{-3}H8	5.0[b] (5.0)					
T_{-4}H6				3.4 (3.4)		
				3.7* (3.7)		
T_{-5}H6	4.8 (3.7)					
T_{-6}H6	3.7[b] (3.7)					
	4.9[c] (5.0)					
T_{-6}H1′	3.6[b] (3.8)					

b. Distances Involving d(CGCAAATTTGCG)$_2$ and **5c** Protons

H2–A_{-7}H2	5.0 (5.0)	H4–A_{-7}H2	5.0 (5.0)	H2–A_6H1′	3.8 (4.8)
CH_3^{R1}–A_6H2″	3.8 (4.6)	H2–T_7H1′	4.3 (4.3)	H3–T_7H1′	4.9 (5.4)
CH_2^{R2}(3)–T_7H2″	2.8 (3.5)	H3–T_8H1′	5.2 (5.4)	CH_2^{R2}(3)–T_8H2″	2.8 (3.3)
CH_2^{R2}(3)–T_8H5′	4.5 (4.7)	H6–T_9H1′	5.0 (5.3)	CH_2^{R2}(2)–T_9H2′	4.4 (4.3)
CH_2^{R2}(3)–T_9H2″	2.8 (3.6)	CH_2^{R2}(3)–T_9H5′	4.5 (4.6)	H3–CH_3^{R4}	3.7 (4.0)
CH_3^{R2}–G_{10}H2′	3.4 (3.4)	CH_3^{R3}–G_{10}H2′	3.4 (3.4)	CH_3^{R3}–CH_3^{R2}	3.4 (3.4)
CH_2^{R2}(2)–CH_2^{n}(4)	2.5 (3.4)	CH_2^{n}(5)–CH_2^{R2}(1)	3.4 (2.9)	CH_2^{R2}(3)–CH_2^{R3}(3)	4.9 (5.1)

[a] In Å, with the same residue. Refined distances are in parentheses. [b] Distances with the $(n-1)$ residue. [c] Distances with the $(n+1)$ residue. Distances marked with asterisks belong to the protons marked with asterisks.

By constraining the dihedral angle ψ_2 between pyrrole rings B and C to be the same as that in the X-ray crystal structure of d(CGCAAATTTGCG)$_2$ with distamycin[7g] (11.1°) and then minimizing, the CHARMm energy of the d(CGCAAATTTGCG)$_2$:**5c** complex greatly increases over that of the unconstrained complex (ψ_2 = 68°). The CHARMm-computed (for gas phase) 35 kcal/mol energy increase is brought about overwhelmingly by differences in the electrostatic energy term (40 kcal/mol) while the contribution from the dihedral energy term is −3 kcal/mol. The difference in CHARMm (gas phase) electrostatic energy terms is dependent upon assumptions of formal charges in the dsDNA:**5c** complex. That the structure with ψ_2 = 68° is electrostatically favored to such a large degree (40 kcal/mol) is due to the assumption that the four aliphatic amino groups of **5c** are protonated (see Discussion). The dihedral constraint of ψ_2 = 11° does not significantly modify the distances between the protons involved in NOE interactions although more of the NOE constraints are met when ψ_2 = 68° (data not shown). The RMS deviation of the d(CGCAAATTTGCG)$_2$ solution structure and the d(CGCAAATTTGCG)$_2$:**5c** solution structure with ψ_2 = 11° was 1.08, whereas, in the case of the DNA:**5c** complex with ψ_2 = 68°, the RMS deviation was 1.29. The molecular contact surface area between the DNA and **5c** was only 2 Å^2 greater when ψ_2 = 11° than when ψ_2 = 68° (Experimental Section).

Dynamic Properties. The signal broadening of the H2, H4, and H6 resonances of **5c** and of the DNA minor groove resonances observed in the 1:1 complex of **5c** with d(CGCAAATTTGCG)$_2$ (Figures 3 and 4) is in accord with minor groove binding.[6e] In the case of the R2 and R3 methyl protons located outside of the groove, the broadening could be due to the relatively slow exchange of **5c** between two equivalent binding sites. Such a change has been proposed for DNA complexes of distamycin[13] and netropsin.[3c,d] In the case of **5c**, a slow movement in the groove due to a sliding motion can be rules out because only one set of **5c** resonances is observed; however, a fast sliding motion is possible. Therefore, the binding-site exchange should be governed by a "flip–flop" mechanism[13] (Scheme III), which does not exclude the existence of a fast sliding motion of **5c** in the minor groove. The equilibrium constant for the formation of the 1:1 complex of **5c** and the hexadecamer d(GGCGCAAATTTGGCGG)/d(CCGCCAAATTTGCGCC) has been determined[8] to be $\sim 10^8$ M^{-1}. From this information, dissociation of **5c** from the

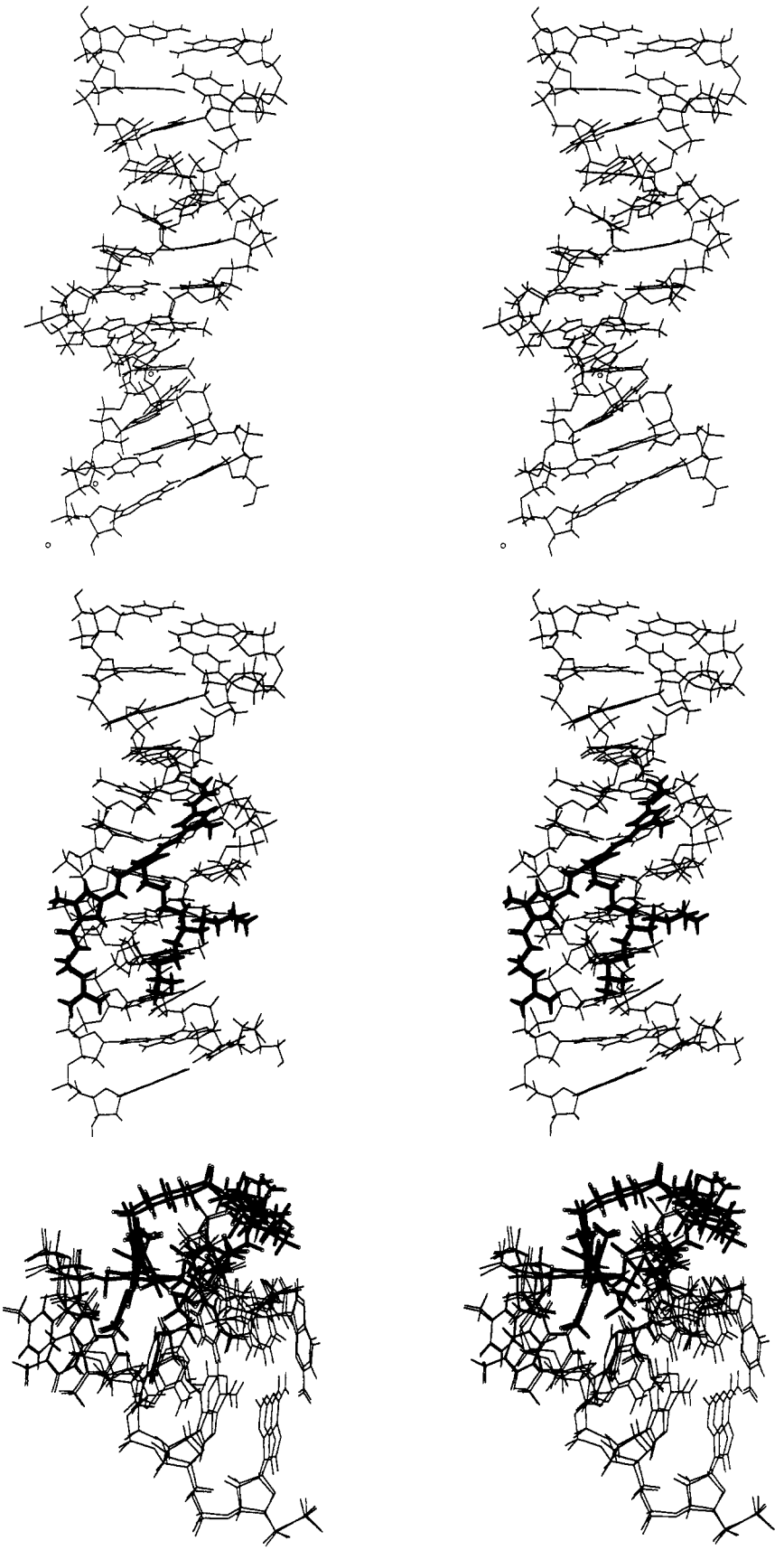

Figure 9. Stereo models of the D_2O solution structures of (top) d(CGCAAATTTGCG)$_2$ and (middle) the 1:1 complex of d(CGCAAATTTGCG)$_2$ with **5c** (ψ_2 = 68°); (bottom) the overlays are two structures of the 1:1 complex of d(CGCAAATTTGCG)$_2$ with **5c** when ψ_2 = 68° and 11°.

hexadecamer is much slower than association. A similar argument should apply to the **5c** complex with d(CGCAAATTTGCG)$_2$ such that one can consider the rate of exchange to be equal to the off-rate ($k_{ex} \cong k_{off}$). In studying the identical line shapes of the diagonal and cross peaks, the rate of exchange for this process was found to be 1.3 s^{-1} (10 °C, Experimental Section), corresponding to an activation energy (ΔG^*) of ca. 17 kcal/mol. A more accurate study of this process would require the determination of the amount of cross-relaxation contributing to the peak intensities and the mixing-time profile,[12] which was not our goal.

Scheme II

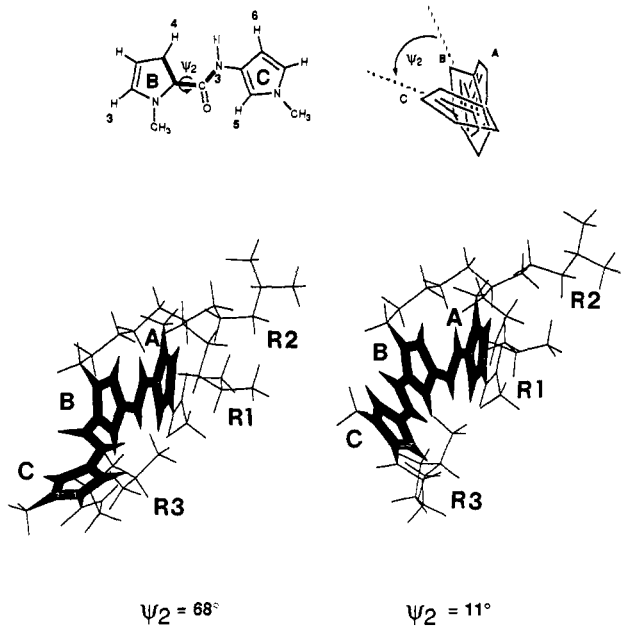

Scheme III

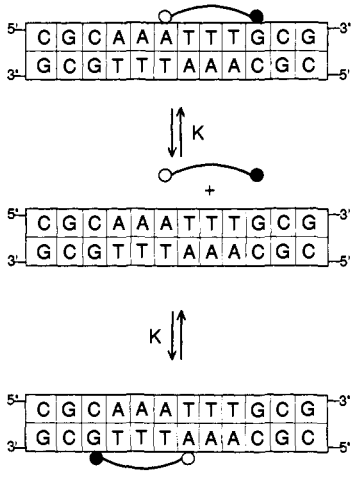

Discussion

The use of 2D NMR spectroscopy and restrained molecular modeling has provided a means for conversion of the crystal structure of d(CGCAAATTTGCG)$_2$ to its solution structure (Figure 9a). The solution structure established the basis for the study of the structure of the 1:1 complex of d(CGCAAATTTGCG)$_2$ with **5c**. ^{1}H NMR cannot resolve resonances that comprise less than 10% of the total population in solutions with molecules as complicated as d(CGCAAATTTGCG)$_2$. Thus, small (and undetectable) populations of the free dodecamer or dodecamer:**5c** complex may exist in forms other than those reported here.

On titration of 1.8×10^{-4} M d(CGCAAATTTGCG)$_2$ with **5c**, the disappearance of the starting A=T imino resonances (Figure 2) and one G≡C resonance at a 1:1 ratio of DNA:**5c** indicates an asymmetrical 1:1 binding. By use of 2D NMR, a better signal/noise ratio is obtained (due to the greater concentration of 3.9 mM), which allows peak shape analysis. The differences in line broadening for the A=T and G≡C imino proton resonances using 2D NMR conditions are consistent with the 1:1 asymmetrical binding of **5c** to d(CGCAAATTTGCG)$_2$. However, **5c** binds differently at pH 7.0 when the size of the oligomer (12 or 16 bp) and the symmetry of the two complementary strands are altered, even if the oligomers contain the same A_3T_3 binding site [d(CGCAAATTTGCG)$_2$ vs d(GGCGCAAATTTGGCGG)/d(CCGCCAAATTTGCGCC)]. The NMR titration of d(GGCGCAAATTTGGCGG)/d(CCGCCAAATTTGCGCC) with **5c** showed a 1:2 complex of dsDNA:**5c** (manuscript in preparation). The difference in binding behavior must be related to the pseudosymmetry of the above hexadecamer and/or to the length of the dsDNA which can lead to a much more flexible minor groove in the A_3T_3 region. The dien polyamine substituent (R2) of **5c** can play an important role in the binding behavior. This observation is in agreement with experiments reported in our previous study.[8b] Determination of equilibrium constants for complexation of two **5c** molecules to a single A_3T_3 minor groove binding site of d(GGCGCAAATTTGGCGG)/d(CCGCCAAATTTGCGCC) by a fluorescence procedure showed cooperative binding with almost 1 order of magnitude separating the first and second association constants (35 °C).[8b]

The two sets of G≡C and A=T Watson–Crick resonances are indicative of an asymmetric binding of **5c** to the d(CGCAAATTTGCG)$_2$ molecule. This binding occurs in the A+T-rich region[8] and results in broadening and downfield shifting of the involved resonances.[16] Assignment of the nonexchangeable protons revealed two sets of DNA resonances but only one set of **5c** resonances. This indicates that the predominant structure involves a single type of asymmetric binding. In some cases in the RM refinement process, long ranges for the NOE-derived constraints were employed. However, the sum of all the distance constraints should lead to one particular position of **5c** with respect to the DNA fragment.

Induced chemical shift differences reveal that the most affected protons involved in the DNA of **5c** interactions are H1′ and H2′2″ (Figure 7). The increase in the number of NOEs observed for H6/8 with CH_3/H5/6/8 protons (not involved in exchange phenomena) can be ascribed to the stiffening of the DNA molecule at the binding site (Table IIIb, see H6/8 interactions with CH_3/H5/6/8) and/or to the dynamic motion of the dsDNA around a position which would bring the aromatic units of the binding site closer together. By convention, we assigned this sequence to the (+) strand. The (-) strand distorts in order to fit the **5c**-bound (+) strand. This is clearly seen in the induced chemical shift differences of H1′ and H2′2″. Reduced electrophoretic mobilities on agarose gels of DNA restriction digest fragments after preincubation with **5c** also suggest a distortion of DNA upon binding to **5c**.[8a] Although the differences in the induced chemical shifts of A_4A_5 and $G_{10}C_{11}$ are generally small, in the case of the terminal base pairs (C_1, G_{-1} and G_{12}, C_{-12}), they are appreciable. For G_{10}H2′, however, the induced chemical shift difference is quite large, enforcing our observation that this proton is involved in an interaction with **5c**. To some small extent, the two base pairs at each end, which hold the double-stranded DNA as a dynamic entity, "sense" the binding process (Figure 7b–d). A small effect on the protons of the aromatic bases suggests that the binding of **5c** does not significantly modify the size of the minor groove, such that only small movements of the base pairs are to be expected. Most changes in the relative position of the aromatic bases occur in the accommodating (-) strand. No effect can be seen on H5′ even though H5″ senses the ligand interaction. The acetamido function (R1) of **5c** affects A_6H5″ while perturbation of C_{11}H5″ is by the (dimethylamino)propyl substituent (R3) on pyrrole ring C. The small effect on T_9H5″ (Figure 7f) suggests that the $(CH_2)_5$ chain which links the tripyrrole peptide to the dien polyamino major groove pointer passes over T_9H5″ at a distance which does not allow perturbation of this proton. These chemical shift differences suggest that, besides the minor groove protons which experience the disruption of the DNA ring currents due to **5c** binding, all the other protons will be affected mainly by the conformational changes of the DNA which take place upon formation of the complex.

(16) Leupin, W.; Chazin, W. J.; Hyberts, S.; Denny, W. A.; Wüthrich, K. *Biochemistry* **1986**, *25*, 5902.

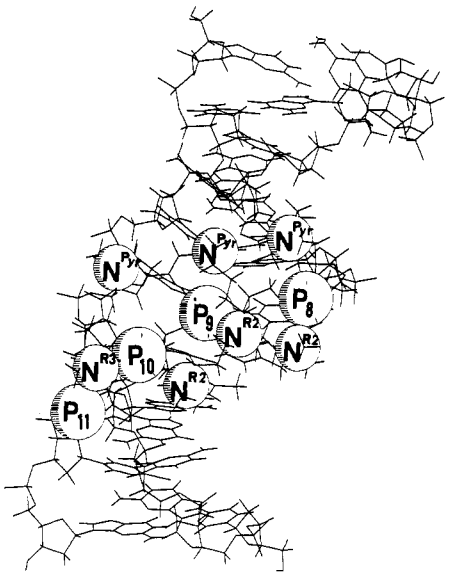

Figure 10. Stick and CPK model of the DNA complex with **5c** showing the pairing of the (+) strand phosphates with the pyrrole and amine nitrogens of **5c**.

Proximities between an *N*-methyl of the dien polyamine substituent (R2) and the *N*-methyl of the (dimethylamino)propyl tail (R3) with $G_{10}H2'$ show that the tail at the carboxyl terminus of **5c** extends out of the minor groove. This requires **5c** to tilt with respect to the minor groove, so that the acetamido end is buried deeper in the minor groove than is the (dimethylamino)-propyl tail. This observation is consistent with the induced chemical shift differences for the R3 protons (Table S1). The methyl of the acetamido moiety (R1) is shielded, while R2 and R3 methyl protons are strongly deshielded, probably due to their proximities with the phosphate backbone. The resonances of the two *N*-methyl substituents on the A and C pyrrole rings do not change due to their noninteractive position. A strong shilding is observed on the first and fourth methylene groups of the $(CH_2)_5$ chain attached to the nitrogen of pyrrole ring B. This suggests that these two methylenes are closest to the DNA phosphates, as shown by the molecular modeling results (Figures 9 and 10). The shielding of the four amide protons of **5c** is position dependent. It is strongest at N1 (see Scheme I and Figure 8) and decreases in going to N3 while that of N4 is slightly deshielded.

Restrained molecular modeling calculations show that there are changes in base pairing and stacking as well as sugar puckering on comparing the DNA:**5c** complex and free DNA. Examination of the X-ray structure of the distamycin/d(CGCAAATTTGCG)$_2$ complex[7g] and the netropsin/d(CGCGAATT^{Br}CGCG)$_2$ complex[7h] leads to the conclusion that the minor groove can increase its width upon binding to lexitropsins. In solution, binding of **5c** increases the width of the minor groove. This is shown by the 0.2–3-Å increase in distances between the phosphates on each side of the minor groove on binding **5c**. The amide nitrogens of **5c** bind 4.5–7 Å from the bottom of the minor groove as **5c** is traced from the acetamide substituent, R1, to the (dimethylamino)propyl substituent, R3. The pyrrolic nitrogen to phosphate distances 5.5–6 and 4–6 Å separate **5c** from the (–) and (+) strands, respectively (Experimental Section). Examination of Figure 10 shows how the positively charged (dimethylamino)-propyl tail (R_3) of **5c** resides at a position which is adjacent to the negative phosphodiester P_{11} on the minor groove side while the protonated triamine moiety is paired with the phosphodiesters P_8, P_9, and P_{10}. All four amino functions of **5c** are located within hydrogen-bonding distances of phosphodiester linkages (NH···O 1.6–2.5 Å). An X-ray structure of d(CGCAAATTTGCG)$_2$ in a complex with distamycin shows that the binding advantage of distamycin is due to the presence of the amidine moiety hydrogen bonded to N3 of A_{-4} at the bottom of the minor groove.[7g] Changing the amidine tail of distamycin to a (dimethylamino)-propyl group and the formamide to acetamide causes a decrease in binding to DNA.[8] However, further change of the *N*-methyl group on its central pyrrole to a dien polyamino side chain (**5c**) will lead to an increased binding as compared to distamycin, which must be due to the indicated electrostatic interactions of the polyamino side chain with the phosphodiester linkages.[2a,8]

A significant structural change can be seen in the amide-linked pyrrole backbone of **5c** upon its binding to the dodecamer. The dihedral angle ψ_2 (Scheme II) of **5c** deviates from planarity by 68° while the same angle in the crystal structure of distamycin in DNA[7g] is only 11° out of the plane of the amide–pyrrole backbone. The structural significance of this deviation in **5c** was examined by fixing ψ_2 at 11° and comparing this structure with the unconstrained solution structure in which ψ_2 is 68°. In determining the merits and faults of each structure, several factors were considered. Helical parameters, calculated with Dickerson's NEWHEL93 program (Experimental Section), for the two minimized complexes were similar when compared to the NMR and crystal distamycin to d(CGCAAATTTGCG)$_2$ complexes (Table V). When $\psi_2 = 11°$, **5c** has 2 Å^2 greater molecular surface contact in the minor groove than when $\psi_2 = 68°$. In contrast, semiempirical calculations (AM1) of the potential energy of the model compound of Scheme II with ψ_2 at 11° and 68° show the latter to be favored by 2.5 kcal/mol (AM1, Figure S10). Both of these differences are small when put into perspective—2.5 kcal/mol is approximately the energy required to break one hydrogen bond (these complexes have nearly 100 hydrogen-bonding interactions), and 2 Å^2 out of 530 Å^2 for the total surface contact area accounts for less than a 0.5% difference in area. The NOE-derived constraints were not quite met to the same degree when $\psi_2 = 11°$ compared to when $\psi_2 = 68°$. Also, the total CHARMm energy when $\psi_2 = 68°$ was considerably lower than when $\psi_2 = 11°$. This is due almost entirely to electrostatic interactions which are difficult to quantify without some knowledge of the extent of protonation of **5c** within the dsDNA:**5c** complex. Nonetheless, of the two conformations of **5c** in the minor groove, the structure with $\psi_2 = 68°$ is likely favored. The dien-microgonotropen **5c** possesses four aliphatic tertiary amino groups, and the extent of their protonation when **5c** is lodged in the minor groove is not obvious. Uncomplexed in solution at pH 7.0, **5c** would have three of the tertiary amino groups protonated while the final amino group would exist as a roughly equimolar mixture of the free base and acid forms.[2a] We have assumed (*vide infra*) in computer modeling that all four tertiary amino functions are fully protonated. When complexed to DNA, the three dien amino groups are intimately associated with three negatively charged phosphates (this is so regardless of whether $\psi_2 = 11°$ or 68°). In separate experiments, minimized structures were created with only two of the three dien amines (plus the (dimethylamino)propyl tail) protonated. In these cases, the electrostatic contribution to the potential energy is decreased by between 40 and 75% depending upon the position of deprotonation. For these structures, the favored values of ψ_2 range from 59° to 77° and conclusions on the structure of the dsDNA:**5c** complex were unchanged.

A comparison of the dynamics of **5c** and distamycin dodecamer complexes reveals the following interesting features. The rate constant for exchange between the two equivalent binding sites (A_3T_3) of the DNA dodecamer d(CGCAAATTTGCG)$_2$ *via* the "flip–flop" mechanism (Scheme III) is 1.3 s^{-1} for **5c** (10 °C) and 0.2 s^{-1} for distamycin (30 °C).[13] Thus, the exchange rate with **5c** at identical A_3T_3 sites appreciably exceeds that for distamycin.

Experimental Section

The synthesis of **5c** has been reported.[8] The self complementary d(CGCAAATTTGCG)$_2$ was obtained by annealing the single-stranded commercially available DNA oligomer (Biomolecular Resource Center, University of California, San Francisco). **The NMR samples** contained

either 0.18 or 3.9 mM double-stranded DNA in 10 mM phosphate buffer and 10 mM NaCl at pH 7.0 (μ = 1.2) with 0.1% TSP in 0.4 mL of D_2O. The 3.9 mM sample, prepared under a nitrogen atmosphere, was lyophilized twice from 99.9% D_2O and once from 99.96% D_2O and was finally dissolved in its original volume of 99.96% D_2O (Aldrich). The solution was kept refrigerated at 4 °C between uses. A weighed sample of **5c** equivalent (in moles) to the DNA was added to this solution as a solid. For the water experiment, the D_2O solvent was removed (Savant Speed-Vac, SC 100) and replaced with an equivalent volume of 10% D_2O in H_2O.

All NMR spectra were recorded at 500 MHz on a GN-500 (General Electric) spectrometer at 10 °C, unless otherwise specified. Chemical shifts were referenced to the signal of TSP (0 ppm). An external lock (D_2O) and a 1–3–3–1 pulse sequence[17a] were used for the H_2O experiment with the 3.9 mM sample of DNA:**5c** complex (25 °C), and an internal lock of 10% D_2O in H_2O was used for the titration experiment (21 °C). The imino resonances were deconvoluted using the GEMCAP program of the GN-500 instrument. **NOESY experiments** were recorded in the phase-sensitive mode using the hypercomplex NOE pulse sequence[17b] with a mixing time of 300 ms for the free DNA (25 °C) and 50, 200, and 400 ms for the DNA:**5c** complex. Spectra were collected into 4K complex points for 512 t_1 increments with a spectral width of 5681 Hz in both dimensions. The data matrix was zero filled to 2 K and apodized with a Gaussian function to give a line broadening of 1 Hz in both frequency domains. **The ROESY experiment** was recorded at 10 °C using the Kessler pulse sequence[16c] with a mixing time of 200 ms and a locking field strength of 3.0 kHz. Here and elsewhere,[3-6,12-15] the numbering of DNA protons follows the rule that the sugar protons will be denoted by prime and double-prime superscripts and preceded by the name of the residue to which they belong. When reference is made to the same proton of more than one residue, all residues are listed followed by the proton type [e.g. $A_6T_7T_8H2''$ means the H2'' (sugar) protons which belong to the A_6, T_7, and T_8 residues; $G_2G_{10}G_{12}H8$ means the H8 (base) protons of the G_2, G_{10}, and G_{12} residues]. When both H2' and H2'' protons are involved in discussion, we used the H2'2'' abbreviation.

Distance calculations were made by measuring the volume integral of the NOE enhancements from the 200 ms NOESY spectrum to which they were related by eq 1, where r_a and r_b are the distances corresponding

$$r_a = r_b(\mathrm{NOE_b}/\mathrm{NOE_a})^{1/6}\ \text{Å} \qquad (1)$$

to the unknown and known (C_3H5–C_3H6, 2.45 Å) interactions of a pair of protons with their corresponding NOE_a and NOE_b.[6b] The linearity of the NOE buildup with τ_m was checked for in the C_3H6–C_3H5 interaction and some other aromatic protons (Figure S9). The exchange rate (k_{ex}) was calculated from eq 2 using the ratio of peak intensities (R), expressed

$$k_{ex} = \ln((1 + R)/2\tau_m(1 - R))\ \mathrm{s^{-1}} \qquad (2)$$

in number of contour levels (off diagonal/diagonal) from a short mixing time (τ_m) NOESY spectrum.[18] The free energy of activation, ΔG^*, for this exchange process at a certain temperature, T (K), was calculated from eq 3.[6d,19]

$$\Delta G^* = 19.14T[10.32 - \log(k_{ex}/T)]\ \mathrm{J/mol} \qquad (3)$$

Computational analysis and restrained molecular modeling were performed on a Silicon Graphics (Mountain View, CA) Iris 4D/340GTX workstation using CHARMm[20] (version 21.3) and QUANTA (version 3.2.3) programs (Polygen/Molecular Simulations, Waltham, MA). The X-ray coordinates employed as a starting point in the creation of the structure of d(CGCAAATTTGCG)$_2$ in water solution were generously provided by C. A. Frederick.[11] The X-ray coordinates to initiate the construction of **5c** were those of distamycin in a complex with d(CGCAAATTTGCG)$_2$, which were taken from the Brookhaven Protein Databank (PDB code: 2DND).[7g] The terminal acetamido and 3-(dimethylamino)propyl groups, the polyamine ligand $N(CH_2CH_2CH_2NMe_2)_2$, and the aliphatic chain $(CH_2)_5$ tethered on the central pyrrole nitrogen of the distamycin backbone were generated using ChemNote and "covalently linked" using 3D Molecular Editor (both functions in the program QUANTA). Atomic partial charges of the atoms in **5c** and the oligomer d(CGCAAATTTGCG)$_2$ were generated from the CHARMm force field's parameter files. All four tertiary amines were modeled as fully protonated with a total charge of +4 for **5c** (partial charge of +0.37 for each proton on a tertiary amine in **5c**).

CHARMm minimization was conducted in vacuo on the crystal structure of d(CGCAAATTTGCG)$_2$ both with and without distance constraints (forces ranged up to 500 kcal/mol·Å^2, depending on the upper and lower limits for a given NOE-derived value) based on nuclear Overhauser effect-calculated distances. All energy values given are CHARMm energies, unless explicitly stated otherwise. In order to attenuate the charge on the phosphate groups, 22 sodium ions were positioned 2.5 Å from each of the partially negative phosphate groups' oxygens, within the O–P–O plane. No added constraints were necessary to prevent the sodium ions from leaving the vicinity (2.5–2.8 Å) of the phosphate oxygens. Energy, nonbonded, and hydrogen-bonded lists were updated every five steps. The nonbonded cutoff distance was 15 Å, and the cutoff distance for hydrogen bonding was 4.5 Å (cutoff angle, 90°). A radially dependent distance dielectric ($\epsilon = R$) was used to account for solvent effects. After 100 steps of steepest descents minimization were performed, approximately 1000 steps of the adopted basis Newton–Raphson algorithm were required to reach a root-mean-square derivative of <0.5 kcal/mol·Å^2. The RMS deviations from the initial crystal structure were compared for the most probable solution and CHARMm-minimized crystal structures.

Initial modeling of the DNA:**5c** complex was performed in QUANTA by interactively docking **5c** into the minor groove of the DNA solution structure (or of the minimized crystal structure for comparison purposes) based on **5c** to oligomer proton contacts indicated from the NOESY experiments. Four sodium ions were removed from the phosphates nearest to where the protonated polyamine side chain and dimethylamine tail of **5c** were initially located. Subsequent minimizations of the olifomer:**5c** complex were conducted exactly as for the oligomer alone (with and without constraints). The RMS deviations to the initial solution DNA structure were compared for the solution complex and CHARMm-minimized complex.

The model compound in Scheme II, comprised of the B and C pyrrole rings of **5c**, was used to study the energy effects that occurred when the dihedral angle ψ_2 (defined in bold lines) was varied. AM1[21] (MOPAC 6.0 package from QCPE, program 455) energies were determined as ψ_2 was rotated in 10-deg increments from 0 to 360° (Figure S10 shows a plot of potential energy vs dihedral angle ψ_2). In addition, ψ_2 was held rigid in single-point calculations at the 68.4° found in the unconstrained solution complex and at the 11.1° found in the crystal complex of distamycin with d(CGCAAATTTGCG)$_2$.[7g] The dihedral angle equivalent to ψ_2 in **5c** was also constrained to 11.1° while the solution complex was CHARMm minimized exactly as previously described for the solution complex without dihedral constraints.

Molecular parameters were measured with QUANTA's "Geometry" function for distances, angles, and dihedrals. Distances reported between atoms have not been reduced by their van der Waals radii. The distances of **5c** to the DNA (–) and (+) strands were measured from the pyrrolic nitrogens to $P_{-4}P_{-5}P_{-6}$ and $P_8P_9P_{10}$, respectively. The depth of **5c** binding was defined by measuring the distances from the amide nitrogens N1, N2, and N3 to the lines connecting $T_{-6}O2$ and A_6H2, $A_{-7}H2$ and T_7O2, and $A_{-8}H2$ and T_8O2 atoms. The extents of solution structural changes of the dodecamers under different conditions were measured in terms of helical parameters[22] with Dickerson's NEWHEL93 program.[23] The bend angle generated in the double-helical axis was calculated from the arcsine of the distance between the two sets of average terminal base pair normal vectors[24] (C_1G_{-1}, G_2C_{-2}, C_3G_{-3} and $G_{10}C_{-10}$, $C_{11}G_{-11}$, $G_{12}C_{-12}$; plotted

(17) (a) Hore, P. J. *J. Magn. Reson.* **1983**, *55*, 283. (b) States, D. J.; Haberkorn, R. A.; Ruben, D. J. *J. Magn. Reson.* **1982**, *48*, 286.

(18) Ernst, R. R.; Bodenhausen, G.; Wokaun, A. *Principles of Nuclear Magnetic Resonances in One and Two Dimensions*; Clarendon Press: Oxford, U.K., 1987.

(19) Günther, H. *NMR Spectroscopy: An Introduction*; John Wiley: New York, 1980; p 241.

(20) Brooks, B. R.; Bruccoleri, R. E.; Olafson, B. D.; States, D. J.; Swaminathan, S.; Karplus, M. *J. Comput. Chem.* **1983**, *4*, 187.

(21) Dewar, M. J. S.; Zoebisch, E. G.; Healy, E. F.; Stewart, J. J. P. *J. Am. Chem. Soc.* **1985**, *107*, 3902.

(22) Saenger, W.; *Principles of Nucleic Acid Structure*; Springer-Verlag: New York, 1984.

(23) NEWHEL93 was generously provided by R. E. Dickerson. The program was run on a VAXstation 3100 with coordinates in Brookhaven's Protein Data Bank format. The best helices were generated from the sugars' C1', the pyrimidine's N1, and the purine's N9 atoms. For more information on an earlier version of this program, see: Prive, G. G.; Yanagi, K.; Dickerson, R. E. *J. Mol. Biol.* **1991**, *217*, 177.

(24) (a) Dickerson, R. E.; Kopka, M. L.; Pjura, P. *Proc. Natl. Acad. Sci. U.S.A.* **1983**, *80*, 7099. (b) Kopka, M. L.; Yoon, C.; Goodsell, D.; Pjura, P.; Dickerson, R. E. *J. Mol. Biol.* **1985**, *183*, 553. (c) Pjura, P.; Grzeskowiak, K.; Dickerson, R. E. *J. Mol. Biol.* **1987**, *197*, 257.

in terms of cosines, Figure S11). The turn angle (deg/bp), axial rise (Å/bp), and helical rise (bp/repeat) were logical output of NEWHEL93 while the pitch height (Å/repeat) was calculated from the product of the helical and axial rises. The molecular contact surface between the two conformations of **5c** and their respective dodecamer conformations was determined using Connolly[25] solvent accessible surface calculations in QUANTA (a radius of 1.4 Å was chosen to simulate a water molecule sized probe). The result of the surface calculation for each DNA:**5c** complex was subtracted from the result for the same DNA with **5c** removed from the binding site. This yielded the surface of that DNA that was inaccessible to the probe due to the presence of **5c** (e.g. the molecular contact surface area).

Acknowledgment. This work was supported by grants from the Office of Naval Research and the NIH. We thank Dr. C. A. Frederick for the use of her X-ray coordinates of d(CGCAAATTTGCG)$_2$ prior to their release.

Supplementary Material Available: Table S1, ^{1}H chemical shifts for **5c**; Figure S1, expanded NOESY spectrum of d(CGCAAATTTGCG)$_2$ in D_2O in the (1.1–3.0) × (1.1–3.0) ppm region; Figure S2, expanded NOESY spectrum of d(CGCAAATTTGCG)$_2$ in D_2O in the (5.5–8.5) × (5.5–8.5) ppm region; Figure S3, expanded NOESY spectrum of d(CGCAAATTTGCG)$_2$ in D_2O in the (1.8–4.6) × (4.6–6.3) ppm region; Figure S4, expanded DQF-COSY spectrum of d(CGCAAATTTGCG)$_2$ in D_2O in the (1.7–3.0) × (4.6–6.3) ppm region; Figure S5, ^{1}H NMR of the imino proton region (experimental, simulated, and deconvoluted) of the 1:1 complex of d(CGCAAATTTGCG)$_2$ at 3.9 mM with **5c** in H_2O; Figure S6, expanded DQF-COSY spectrum of the 1:1 complex of d(CGCAAATTTGCG)$_2$ with **5c** in D_2O in the (1.4–3.1) × (1.4–3.1) ppm region; Figure S7, expanded NOESY spectrum of the 1:1 complex of d(CGCAAATTTGCG)$_2$ with **5c** in D_2O in the (1.0–4.5) × (1.0–4.5) ppm region; Figure S8, expanded ROESY spectrum of the 1:1 complex of d(CGCAAATTTGCG)$_2$ with **5c** in D_2O in the (0.1–4.8) × (5.2–9.8) ppm region; Figure S9, NOE volume integrals vs mixing time for some interactions in the **5c**:DNA complex; Figure S10, AM1 reaction coordinate for potential energy vs dihedral angle ψ_2 (Scheme II) as ψ_2 is varied in 10-deg increments from −180 to +180°; and Figure S11, normal vector plots to the mean plane of the base pairs of each of the dodecamer structures described in Table V showing the bends of the helical axes (17 pages). Ordering information is given on any current masthead page.

(25) Connolly, M. L. *Science* **1983**, *221*, 709.